Macromolecules
ARTICLE

Coarse-Grained Molecular Dynamics Simulation of Polyethylene Terephthalate (PET)

Qifei Wang,[†] David J. Keffer,*,[†] Donald M. Nicholson,[‡] and J. Brock Thomas[§]

[†]*Department of Chemical and Biomolecular Engineering, University of Tennessee, Knoxville, Tennessee 37996, United States,* [‡]*Computer Science and Mathematics Division, Oak Ridge National Laboratory, Oak Ridge, Tennessee 37830-8026, United States, and* [§]*Eastman Chemical Company, Kingsport, Tennessee 37662-5230, United States*

ABSTRACT: A coarse-grained (CG) model of poly(ethylene terephthalate) (PET) was developed and implemented in CG molecular dynamics (MD) simulations of PET chains with degree of polymerization up to 50. The CG potential is parametrized to structural distribution functions obtained from atomistic simulations [*J. Phys. Chem. B* **2010**, *114*, 786] using an inversion procedure based on the Ornstein−Zernike equation with the Percus−Yevick approximation (OZPY) [*Phys. Rev. E* **2010**, *81*, 061204]. The CGMD simulation of PET chains satisfactorily reproduces the structural and dynamic properties from atomistic MD simulation of the same systems. We report the average chain end-to-end distance and radius of gyration, relaxation time, self-diffusivity, and zero-shear-rate-viscosity's dependence on degree of polymerization. For the longest chains, we find the scaling exponents of 0.51, 0.50, and −2.00 for average chain end-to-end distance, radius of gyration and self-diffusivity, respectively. The exponents are very close to the theoretical values of entangled polymer melt systems (0.50, 0.50, and −2.0). The study of entanglement in the longer chains shows that the tube diameter, number of monomers between entanglement points and interentanglement strand length are in close agreement with the reported values for an entangled PET melt.

1. Introduction

Poly(ethylene terephthalate) (PET) is one of the most important engineering plastics and is widely used in packaging industry as bottles, fibers, and packaging films. The macroscopic structural and dynamic properties of PET have been widely studied through experiments. The computational studies of structural and dynamic properties of PET are limited due to the fact that the polymer's physical properties depend on several time and length scales,[1] which require multiscale modeling techniques.

Molecular-level simulation has proved to be a useful computational technique to study structural, physical and transport properties of polymers of short length. The structural and transport properties have been studied via molecular simulation with different force fields. Hedenqvist et al.[2] developed an atomistic model for PET (hereafter referred to as the HBB model). The specific volume, solubility parameters and dipolar correlation factors obtained from (MD) simulation using this model are in good agreement with the experimental results. Implementing the HBB model for PET in MD simulations of a single chain with 60 monomers, Bharadwaj[3] further studied the diffusion of methane in amorphous PET. Boyd et al. modified the torsion component of the HBB potential to satisfy chain dynamics and relaxation.[4] Using a modified HBB model, Wang et al.[5] studied the structural, thermodynamic and transport properties of PET oligomers of 125 chains with degree of polymerization (DP) varying from 1 to 10 each. Kamio et al.[6] generated structural properties needed to obtain the CG potentials. Other models used in the molecular simulation of PET include the polymer-consistent force field (PCFF) model,[7] the open force-field (OFF) model,[8] the rotational isomeric state (RIS) conformational model,[9−11] and a

more recently developed model.[12] All of these studies involve either a single chain or chains with a degree of polymerization (DP) less than or equal to 20. However, the time and length scales used in molecular simulation are far below that of real long chain polymer systems. With finite computational resources, it is beyond current computational capabilities to use an atomistically detailed simulation technique to obtain long time trajectories of long chains. For example, to determine the self-diffusivity of long polymer chains, the simulation must reach the long-time limit required by the Einstein relation. The simulation time can easily be on the order of microseconds or milliseconds and the corresponding real time for the computation is on the order of years or decades.

The motivation behind a coarse-grained (CG) procedure is to lift these computational limitations by eliminating some degrees of freedom in the simulation in exchange for computational efficiency. The reduction in the degrees of freedom is accomplished by grouping atoms in certain fragments of the chain into "superatoms", which interact with their own CG potential.[6,13] Since the degrees of freedom are greatly reduced in the CG model and softer CG potentials are often obtained,[13] larger length and time scales can be reached in the CG level simulation. Structural and transport properties can be calculated directly by CG simulation.[14] Furthermore, the CG level properties can be mapped back to the molecular level through the use of scaling factors.[13−15] This multiscale modeling technique has been used in the study of structure and dynamics of biomacromolecules[16,17] and polymer chain molecules (polysterene (PS),[13,18,19] poly(methyl methacrylate) (PMMA),[14] polyethylene (PE),[20] poly(ethylene oxide) (PEO),[14,21,22] polyisoprene/polystyrene blend,[23,24] bisphenol A polycarbonate (BPA-PC)[25] and azobenzene liquid crystal[26]). Although the molecular simulation of PET has a long history, the CG simulation of PET is less prevalent in the literature.

*Author to whom correspondence should be addressed. E-mail: dkeffer@utk.edu.

Published on Web 11/19/2010

Kamio et al.[6] performed CG end-bridging Monte Carlo simulations of PET melts, generating equilibrium structural and entanglement properties. This current work is aimed at conducting CGMD simulations to investigate the structural and dynamic properties of PET chains with a DP up to 50. This range of DP is relevant because PET leaving an industrial finishing reactor possesses a DP in the 30–50 range.

There is an up front price that must be paid for the computational efficiency of the CG procedure; the price is the development of an accurate interaction potential for the CG superatoms. Obtaining reliable nonbonded interaction potentials is particularly challenging. Two common methods have been adopted to obtain nonbonded CG potentials, namely adjusting power law type potential parameters (Lennard-Jones 12–6, 7–6, 7–4, 7–5),[13,18,19,26] and iterative Boltzmann inversion method.[6,27] CG level simulations have been conducted using CG potentials from both of the above methods. Using CGMD simulation with power law type of nonbonded potential, Harmandaris et al.[13,18,19] studied structural and dynamic properties of long chain polystyrene (PS) systems. A scaling factor is reported for the speed up of chain dynamics based on the difference on mean square displacements. Using potentials from the iterative Boltzmann inversion[27] method, Kamio et al.[6] performed CG end-bridging Monte Carlo simulations of PET melt. Both methods used to obtain CG potentials need improvements with respect to computational accuracy and efficiency.[16,26,28,29]

Alternative methods have been developed recently to improve computational accuracy and efficiency of the CG procedure. Fritz et al.[30] recently present a new approach that obtains both the bonded and nonbonded interactions of the CG model of PS from the sampling of isolated atomistic chains and pairs of oligomers in vacuum. The method is computationally inexpensive. The CG model of PS using the calculated CG potentials reproduces the melt packing, the density and local chain conformations of atactic as well as stereoregular PS.

The Ornstein–Zernike integral equation (IE) theory[31,32] is also widely used to study the structural properties of polymer systems.[28,33–36] In most cases, the IE theory is used to generate structural properties like pair correlation functions (PCFs) given the interaction potential. Although, it has been used to obtain the nonbonded potential parameters,[37] the iterative nature of the procedure limits the computational gain from coarse-graining. Noniterative procedures also exist in which structural properties and interaction potentials can also be obtained from the theory and a description of the atomistic system.[34–36]

An alternative procedure based on the Ornstein–Zernike equation with the Percus–Yevick approximation (OZPY equation)[38,39] is to extract the CG nonbonded potential from the PCFs, which is referred as inverse OZPY or OZPY^{-1}. The use of OZPY^{-1} method[40] to obtain the interaction potential has been reported in the study of monatomic systems.[41–44] The OZPY^{-1} method is approximate only because of the approximate nature of the PY assumption for the direct correlation function. On the other hand, it is simple and fast compared to the current methods of comparable accuracy. Wang et al.[29] demonstrated that this method can be applied to systems that have intramolecular degrees of freedom, such as the diatomic Lennard-Jones fluid. Here, we apply the OZPY^{-1} method to extract nonbonded CG potential for PET chains with PCFs from atomistic MD simulations.

In previous work,[5] atomistic simulations of PET oligomers of degree of polymerization 1, 2, 3, 4, 6, 8, and 10, using the HBB model were performed. For the tetramer, hexamer, octamer, and decamer, PCFs (based on center of mass position of the CG beads), relaxation times, and diffusion coefficients from these simulations were obtained. In this work, we use the structural results from the atomistic simulations of PET as input into the OZPY^{-1} method to generate a CG potential of PET. We perform

CGMD simulations of longer chain PET with DP equal to 4, 6, 8, 10, 20, 30, 40, and 50. Structural and transport properties are studied at the CG level and mapped back to molecular level. Finally, the entanglement of long chain systems are studied by the Z algorithm.[45] This paper is organized as follows. The details of the potential and simulation techniques are given in section 2. The Results and Discussion are presented in section 3. Conclusions are listed in section 4.

2. Simulation Method

2.1. Atomistic Simulation of PET Tetramer, Hexamer, Octamer, and Decamer. Although no additional atomistic simulations were performed for this work beyond those previously reported,[5] this work does present new properties from the atomistic simulations. Therefore, we briefly review the simulation procedure that was used in the previous work,[5] where a more detailed description is provided. We use the modified anisotropic united atom HBB potential model developed by Hedenqvist, Bharadwaj, and Boyd[2,4] for PET to describe the intramolecular and intermolecular potential of oligomers molecules. We simulated in the isobaric–isothermal (NpT) ensemble and implemented the Hamiltonian-based thermostat and barostat of Keffer et al.[46] with controller frequencies set to 10^{-4} fs. The XI-RESPA NPT algorithm developed by Tuckerman et al.[47] was used to integrate the equations of motion. The large time step was 2 fs and the small time step was 0.2 fs. The parallel code we used was built in-house and is written in FORTRAN-90, using MPI for interprocessor communication. It has been tested rigorously across a variety of applications. For the simulations in this work, we verified conservation of the Hamiltonian in order to validate our choices of time step, cutoff distance and to minimize the possibility of bugs in the potential. For DP from 4 to 10, we simulated 125 molecules. The state point was set at 0.13 kPa and 563 K, as this corresponds to conditions within a finishing reactor.[48] As for the initial conditions, we estimated the initial density and placed the particles in the simulation volume, avoiding significant overlap. To accelerate equilibration, we started with a higher temperature. Then we gradually decreased the temperature of the system and equilibrated to the correct density. Typically, each equilibration stage lasted for 1 ns. The details of the equilibration procedure can be found in elsewhere.[2,5,6] Data production followed and lasted over 30 ns for the octamer and decamer. These lengths of data production were chosen to be greater than the longest rotational relaxation time as determined in the simulation.

2.2. CGMD Simulations of Longer PET Chains with DP = 4, 6, 8, 10, 20, 30, 40, and 50. We propose that PET can be modeled at a coarse-grained level with two spherical beads of type A and B. The A bead corresponds to the benzene fragment, C_6H_4, and the B bead corresponds to all of the atoms between benzene fragments, $C_4H_4O_4$. In the construction of the PCFs involving A and B from the atomistic simulations, the A and B beads are placed at the center-of-mass of the atoms in the corresponding fragment, as shown in Figure 1. This definition introduces a small error due to end effects in the B beads terminating each chain, which in the atomistic simulation are actually $C_3H_5O_3$. This mapping scheme contains a reduction in the number of degrees of freedom that enhances computational efficiency making the study of the dynamics of longer-chains tractable, while at the same time keeping sufficient structural details to reproduce the atomistic chain conformations. The validation of this choice of mapping scheme is given in the Results and Discussion.
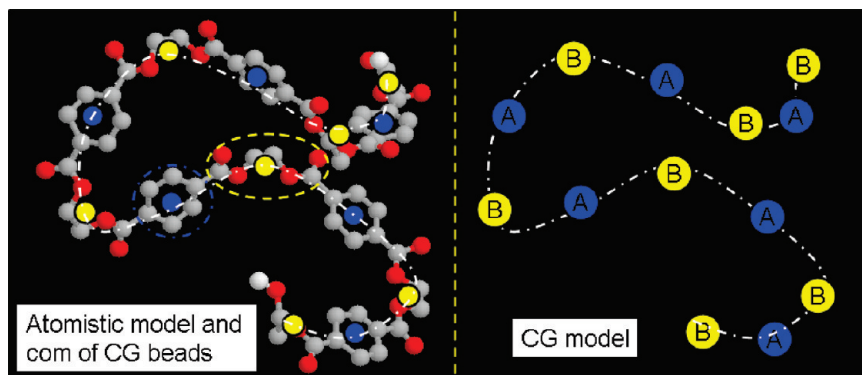
Figure 1. Molecular and CG models of the PET hexamer molecule. Molecular model and center of mass (com) position of CG beads are shown the left. CG model is shown on the right.

The CG potential includes bond stretching (BA), bond bending (BAB and ABA), bond torsion (BABA), intramolecular nonbonded interactions (for beads over four bonds), and intermolecular nonbonded interactions (BB, BA, and AA). Probability distribution functions (PDFs) for stretching, bending, torsion, and nonbonded interactions between CG particles were generated from the atomistic simulations. In the development of coarse-grained (CG) potentials, for the stretching, bending and torsion modes, there are straightforward approximations that relate the interaction potential directly to the PDFs.[13] The effective interaction potential between a particle of type α and a particle of type β, $\varphi_{\alpha\beta}$, as a function of the separation between particles, r, can be related to the probability distribution function, $g_{\alpha\beta}(r)$, via

$$\varphi_{\alpha\beta}(r) = -k_B T \ln(g_{\alpha\beta}(r)) + c_{\alpha\beta} \qquad (1)$$

where k_B is Boltzmann's constant, T is temperature, and $c_{\alpha\beta}$ is a constant. Note here coordinates need to be changed for the bending (from r to θ (bending angle)) and torsion (from r to ϕ (torsion angle)) modes.[13,18,26]

To extract the nonbonded CG potentials, there are two major methods currently used. First, the parameters of an analytic potential such as Lennard-Jones are adjusted to closely reproduce the target PCF in the atomistic liquid/melt. A problem with this method is that the difference of conformations and orientations between fragment molecules and target molecules may not be reflected correctly on the corresponding coarse-grained potentials.[16,26] For example, the conformations of phenol rings in liquid benzene and that in PS melt where the rings are embedded into a long chain may be different. Consequently, these conformations would be misrepresented in the CG potential. The calculated potentials cannot be used under ambient pressure condition or be applied to study the formation of ordered structures driven by enthalpic interactions.[30] Fritz et al.[30] recently developed a new method that addresses these drawbacks. The method derives nonbonded potentials from constraint dynamics with the all−atom model of two trimers (or tetramers) of PS in vacuum. In this way, the atomistic melt properties are not used in the parametrization while the potential can still be used in the condensed melt phase. To some extent, the multibody contributions to the effective potential are taken into account.

In the second method, a tabulated potential is numerically determined by simulation iteration. The interaction potential is refined iteratively via

$$\varphi_{\alpha\beta, i+1}(r) = \varphi_{\alpha\beta, i}(r) + k_B T \ln\left(\frac{g_{\alpha\beta, i}(r)}{g_{\alpha\beta}(r)}\right) \qquad (2)$$

where $g_{\alpha\beta}(r)$ is the target PCF. Potentials obtained from this procedure will closely reproduce the CG atomistic liquid PCFs. The challenging part of this method is obtaining PCFs from simulations in each iteration. As mentioned by Guenza,[28] those simulations have to be performed on length scales and time scales large enough to ensure a reliable numerical predictions of the potential at the length scale characteristic of the coarse-graining procedure. This could strongly limit the computational gain of CG procedure.

In this work, we use the form of the bonded potentials from eq 1 and nonbonded potentials from the $OZPY^{-1}$ method to describe both the intramolecular and intermolecular potential of CG PET chains. The Ornstein−Zernike integral equation for a mixture of simple fluids[38] is

$$g_{\alpha\beta}(r,r') - 1 = c_{\alpha\beta}(r,r')$$
$$+ \sum_{\gamma} \int c_{\alpha\gamma}(r,r'') n_{\gamma}(r'') [g_{\gamma\beta}(r'',r') - 1] \, d^3 r'' \qquad (3)$$

where the pair correlation function between particles of type α and β located respectively at r and r', $g_{\alpha\beta}(r,r')$, is related to the direct correlation, $c_{\alpha\beta}(r,r')$, and an integral including the interactions of the α and β particles with a third particle, γ, located at r'' with a singlet density, $n_{\gamma}(r'')$. There is a summation over γ spanning all types of particles. This equation in its present form implicitly allows for a different interaction potential between each pair of types of particles. In essence, the summation over γ is a summation over interaction potentials. To emphasize this, the Percus−Yevick approximation of the direct correlation function can be written as

$$c_{\varphi_i}(r,r') = g_{\varphi_i}(r,r') \left[1 - \exp\left(\frac{\varphi_i(r,r')}{k_B T}\right)\right] \qquad (4)$$

Substitute this to OZ equation yields the OZPY equation[29]

$$y_{\varphi_1}(r) = 1 + \sum_{\varphi_2} \sum_{\varphi_3} \frac{2\pi n}{r} \int_0^{\infty} ds \, s[h_{\phi_2}(s)$$
$$- y_{\phi_2}(s) + 1] \int_{|r-s|}^{r+s} dt \, th_{\varphi_3}(t) \qquad (5)$$

With the definition of cavity function[49] and total correlation function respectively as

$$y_{\varphi_i}(r,r') = g_{\varphi_i}(r,r') \exp\left(\frac{\varphi_i(r,r')}{k_B T}\right) \qquad (6)$$

$$h_{\varphi_i}(r,r') = g_{\varphi_i}(r,r') - 1 \qquad (7)$$

Table 1. Unscaled Structural, Thermodynamic and Transport Properties of PET with Different DP from CGMD Simulations (for DP = 4, 6, 8, 10, 20, 30, 40 and 50) at p = 0.13 kPa, T = 563 K

DP	4	6	8	10	20	30	40	50
N	125	125	125	125	125	125	125	125
ρ^* (g/cm³)	1.22 ± 0.03	1.29 ± 0.01	1.29 ± 0.01	1.29 ± 0.01	1.18 ± 0.02	1.20 ± 0.01	1.25 ± 0.02	1.24 ± 0.01
D^* (10^{-10} m²/s)	2.71 ± 0.2	0.76 ± 0.15	0.47 ± 0.13	0.32 ± 0.06	0.16 ± 0.03	0.08 ± 0.02	0.045 ± 0.022	0.025 ± 0.01
η^* (10^{-2} Pa·s)	0.1 ± 0.01	0.26 ± 0.09	0.41 ± 0.09	0.43 ± 0.04	0.44 ± 0.03	0.65 ± 0.13	1.50 ± 0.17	2.31 ± 0.40
$\langle R_{ete} \rangle^*$ (Å)	17.5 ± 6.2	22.1 ± 7.8	24.7 ± 9.1	28.3 ± 10.2	44.2 ± 15.9	56.6 ± 21.0	63.0 ± 23.0	69.8 ± 22.7
$\langle R_g \rangle^*$ (Å)	8.1 ± 1.7	9.5 ± 5.4	10.5 ± 6.3	12.2 ± 6.4	19.6 ± 7.0	24.7 ± 9.1	28.0 ± 7.7	30.9 ± 10.6
τ_R^* (ns)	0.96	3.04	4.69	10.33	51.28	128.20	476.25	909.10
τ_{KWW}^* (ns)	0.56	2.34	3.99	7.88	34.39	95.05	491.21	1006.81
β_{KWW}^*	0.92	0.84	0.86	0.81	0.75	0.70	0.61	0.58
kinetic energy* (aJ/bead) $\times 10^{-2}$	1.16 ± 0.04	1.16 ± 0.02	1.17 ± 0.02	1.17 ± 0.02	1.17 ± 0.02	1.17 ± 0.02	1.17 ± 0.03	1.16 ± 0.06
bonded energy* (aJ/bead) $\times 10^{-2}$	0.92 ± 0.03	1.06 ± 0.02	1.11 ± 0.02	1.14 ± 0.02	1.19 ± 0.01	1.21 ± 0.02	1.22 ± 0.01	1.22 ± 0.04
nonbonded energy* (aJ/bead) $\times 10^{-3}$	−1.24 ± 0.03	−1.23 ± 0.06	−1.18 ± 0.09	−1.18 ± 0.04	−1.25 ± 0.04	−1.21 ± 0.03	−1.20 ± 0.03	−1.21 ± 0.03

where φ_1 is always the unknown nonbonded potential, while the summations of φ_2 and φ_3 include both nonbonded and bonded potentials. Conceptually, then we measure all $h_{\varphi_i}(t)$ in the simulation and we solve eq 5 numerically for $y_{\varphi_1}(r)$ from which the potential can be directly extracted. The details of the application of the OZPY^{-1} method to polyatomic fluid is given as Supporting Information of this paper. The method requires a meticulous accounting of the allowable combinations of interaction potentials in the summations of φ_2 and φ_3, which are dependent on the connectivity of the polymer chain. For example, for the diatomic molecule, there were three combinations of φ_2 and φ_3 (stretching−nonbonded, nonbonded−stretching, and nonbonded−nonbonded). One cannot have stretching−stretching in a diatomic system. For PET, there are 34 such combinations. All the calculated potentials are presented in the Discussion.

In addition to CG model and potentials, we also require reliable initial configurations to start the CGMD simulation. For DP = 4, 6, 8, and 10, the initial configurations of CG chains are based on center of mass positions of the fragments from the atomistic simulations. For DP = 20, 30, 40, and 50, we estimated the initial density and placed the particles in the simulation volume carefully with proper bond length and angles, then gradually introduced the nonbonded interactions to avoid overlap.

We again simulated in the isobaric−isothermal (NpT) ensemble under the same pressure and temperature as the atomistic simulation. The time steps of CGMD simulation are 10 times larger than those used in the atomistic MD simulation. The simulation method is similar to that used in the atomistic MD. After an equilibrium stage, the systems reach the equilibrium densities. The equilibrium densities of different systems are in the range of 1.18 to 1.29 g/cm³, which is close to the finding of Kamio et al.[6] by a different method. End effects exist but become smaller with increasing chain length.

Apparent speed up is observed in CG level simulation. On the basis of wall-clock time, the CGMD simulations are about 50 times faster than the atomistic simulations. Note here that in our atomistic simulations, a united-atom model was used for hydrogen bound to carbon, already eliminating some degrees of freedom. The speed up factor would be larger if the hydrogens were explicitly accounted for in the atomistic simulation. The procedure is still computationally intensive, to finish a run of 4300 ns for a system of chains with DP of 50, it took roughly 3 months on 16 processors. However, such a run would have been infeasible with atomistic simulation. The duration of data production was chosen to be 4 or 5 times the longest rotational relaxation time as determined in the simulation for DP from 4 to 30. These simulations ran as long as 1600 ns. For DP equal to 40 and 50, the simulation times were 2800 and 4300 ns respectively, which are roughly equal to the longest relaxation times of these systems, which represents a compromise based on finite computational resources.

3. Results and Discussion

In this section, we present the results of the CGMD simulations for PET with DP = 4, 6, 8, 10, 20, 30, 40, and 50. For the four shortest chains, we compare the results with those of the corresponding atomistic simulations. The results are broken into three parts: structural properties, transport properties and entanglement analysis. A summary of raw properties generated from the CGMD simulations is presented in Table 1. Note that these properties have not been adjusted by any time or length scaling factors. When mapping the CGMD simulation results back to the molecular level, scaling factors based on the time scale difference of the two level simulations are used.[13,25] A comparison of structural and dynamic properties from atomistic MD simulation and corresponding scaled values from CGMD simulation for DP equals 4, 6, 8, and 10 are listed in Table 2. All the time related properties in the figures (end-to-end autocorrelation functions, self-diffusivity, mean square displacement and zero-shear-rate viscosity) are scaled with the appropriate time-scaling factor. A detailed explanation of each scaling factor is contained in the discussion of its related property. In the sections below, our discussion is largely confined to comparison between the atomistic MD and CGMD simulations, as well as comparison of the observed results with the Rouse and reptation theories. Comparison of the results of the atomistic simulations with experimental measurements, which was in general quantitative, is available elsewhere.[5]

3.1. Structural Properties. In Figure 2, we show the distributions of bonded and nonbonded CG beads obtained from atomistic simulations. These distribution functions are based on the analysis of configurations from atomistic MD of the tetramer, hexamer, octamer and decamer. As shown in Figure 1, these distribution functions are calculated according to the center of mass position of CG beads. In our CG model, there is only one type of stretching mode (BA), two types of bending modes (BAB and ABA) and three types of nonbonded modes (BB, BA, and AA). The stretching mode shows a Gaussian type distribution with the equilibrium bond distance around 5.0 Å. The bending BAB shows single peak centered at 150°, while the bending ABA displays bimodal distribution with one peak centered at 110°, the other centered at 170°. The torsional mode distribution is similar to that of Kamio et al.'s work,[6] although they used a different CG model. Similar features for stretching and bending

Table 2. Comparison of Structural, Thermodynamic, and Transport Properties of PET from Atomistic MD Simulation DP = 4, 6, 8, and 10 and CGMD Simulations for all DP at p = 0.13 kPa, T = 563 K[a]

DP	simulation method	ρ (g/cm^3)	D (10^{-10}m^2/s)	η (10^{-2}Pa·s)	$\langle R_{ete} \rangle$ (Å)	$\langle R_g \rangle$ (Å)	τ_{KWW} (ns)	kinetic energy (aJ/bead) × 10^{-2}	bonded energy (aJ/bead) × 10^{-2}	nonbonded energy (aJ/bead) × 10^{-2}
		1.0	0.186	5.38	1.0	1.0	7.5	1.0	1.09	16.35
4	atomistic MD	1.29 ± 0.01	0.40 ± 0.09	0.65 ± 0.07	21.1 ± 7.5	8.9 ± 5.2	5.6	1.17 ± 0.01	1.14 ± 0.01	−2.12 ± 0.01
	CGMD-scaled	1.22 ± 0.03	0.50 ± 0.02	0.54 ± 0.06	17.5 ± 6.2	8.1 ± 1.7	5.5	1.17 ± 0.04	1.00 ± 0.04	−2.05 ± 0.04
6	atomistic MD	1.29 ± 0.01	0.17 ± 0.02	1.95 ± 0.65	26.8 ± 10.2	11.2 ± 4.4	15.8	1.16 ± 0.01	1.15 ± 0.01	−2.00 ± 0.01
	CGMD-scaled	1.29 ± 0.01	0.14 ± 0.01	1.40 ± 0.48	22.1 ± 7.8	9.48 ± 5.4	17.4	1.16 ± 0.03	1.15 ± 0.03	−2.05 ± 0.11
8	atomistic MD	1.29 ± 0.01	0.10 ± 0.01	2.23 ± 0.60	28.6 ± 11.2	12.5 ± 5.3	25.3	1.17 ± 0.07	1.15 ± 0.07	−1.94 ± 0.02
	CGMD-scaled	1.29 ± 0.01	0.09 ± 0.01	2.21 ± 0.48	24.7 ± 9.1	10.49 ± 6.3	26.8	1.17 ± 0.02	1.21 ± 0.02	−1.91 ± 0.12
10	atomistic MD	1.29 ± 0.01	0.07 ± 0.01	3.03 ± 0.80	34.2 ± 9.4	13.2 ± 3.8	38.6	1.17 ± 0.06	1.15 ± 0.06	−1.90 ± 0.01
	CGMD-scaled	1.29 ± 0.01	0.06 ± 0.01	2.31 ± 0.16	28.3 ± 10.2	12.18 ± 6.4	59.1	1.16 ± 0.02	1.24 ± 0.02	−1.93 ± 0.08
20	CGMD-scaled	1.18 ± 0.02	0.030 ± 0.006	2.37 ± 0.16	44.2 ± 15.9	19.6 ± 7.0	257.9	1.17 ± 0.02	1.30 ± 0.01	−2.04 ± 0.07
30	CGMD-scaled	1.20 ± 0.01	0.015 ± 0.004	3.50 ± 0.70	56.6 ± 21.0	24.7 ± 9.1	712.9	1.17 ± 0.02	1.32 ± 0.02	−1.98 ± 0.05
40	CGMD-scaled	1.25 ± 0.02	0.008 ± 0.004	8.07 ± 0.91	63.0 ± 23.0	28.0 ± 7.7	3684.0	1.17 ± 0.03	1.33 ± 0.01	−1.96 ± 0.05
50	CGMD-scaled	1.24 ± 0.01	0.005 ± 0.002	13.37 ± 2.2	69.8 ± 22.7	30.9 ± 10.6	7551.0	1.16 ± 0.06	1.33 ± 0.04	−1.98 ± 0.05

[a] Properties from CGMD simulation have been scaled with scaling factors listed for each property in the second row.
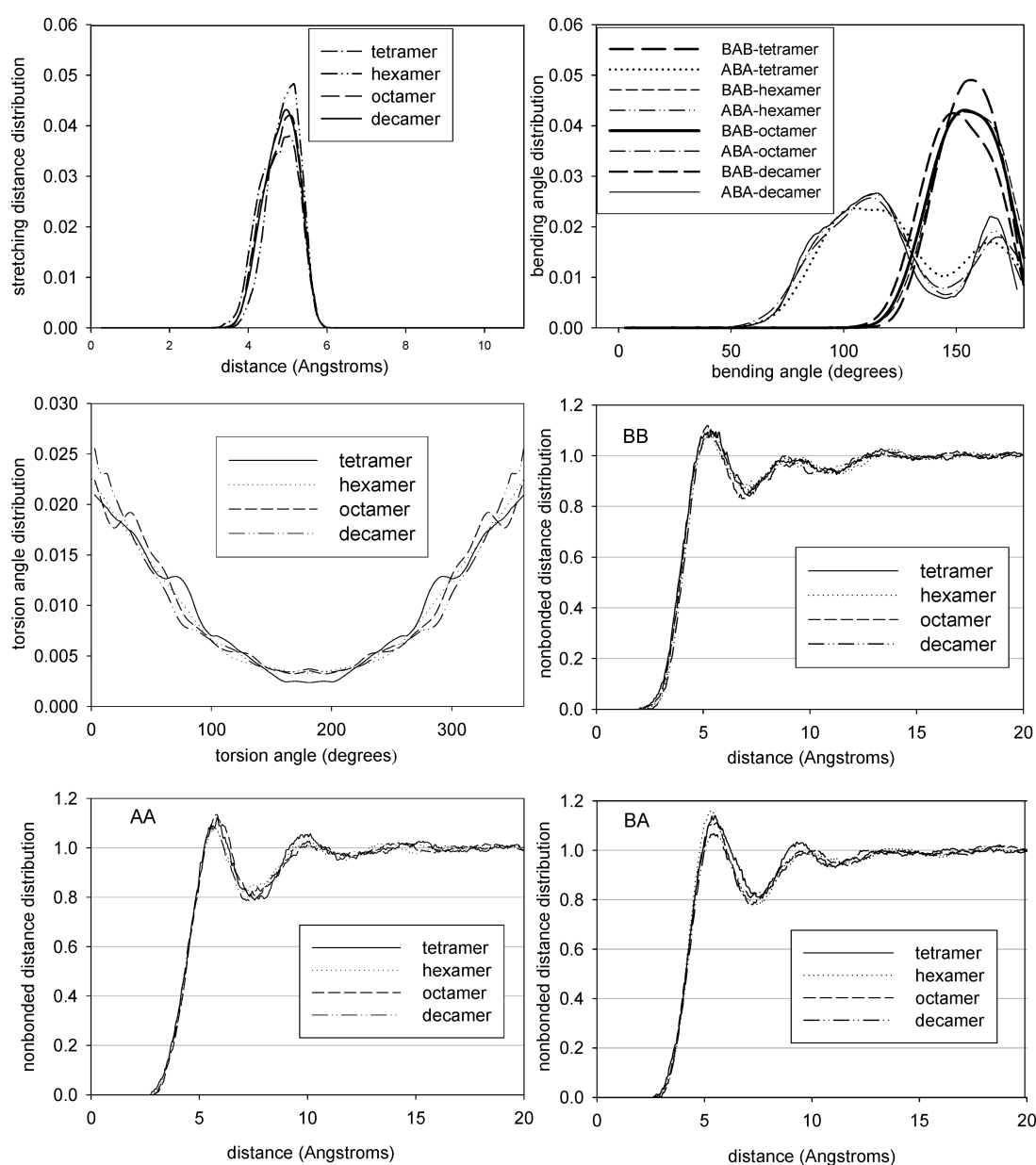
Figure 2. Bonded (stretching, bending, and torsion) CG probability distribution functions (PDFs) and nonbonded CG pair correlation functions (PCFs) of tetramer, hexamer, octamer and decamer. PCFs are based on the center of mass position of the CG beads, obtained by analyzing the atomistic MD simulations of these oligomers.
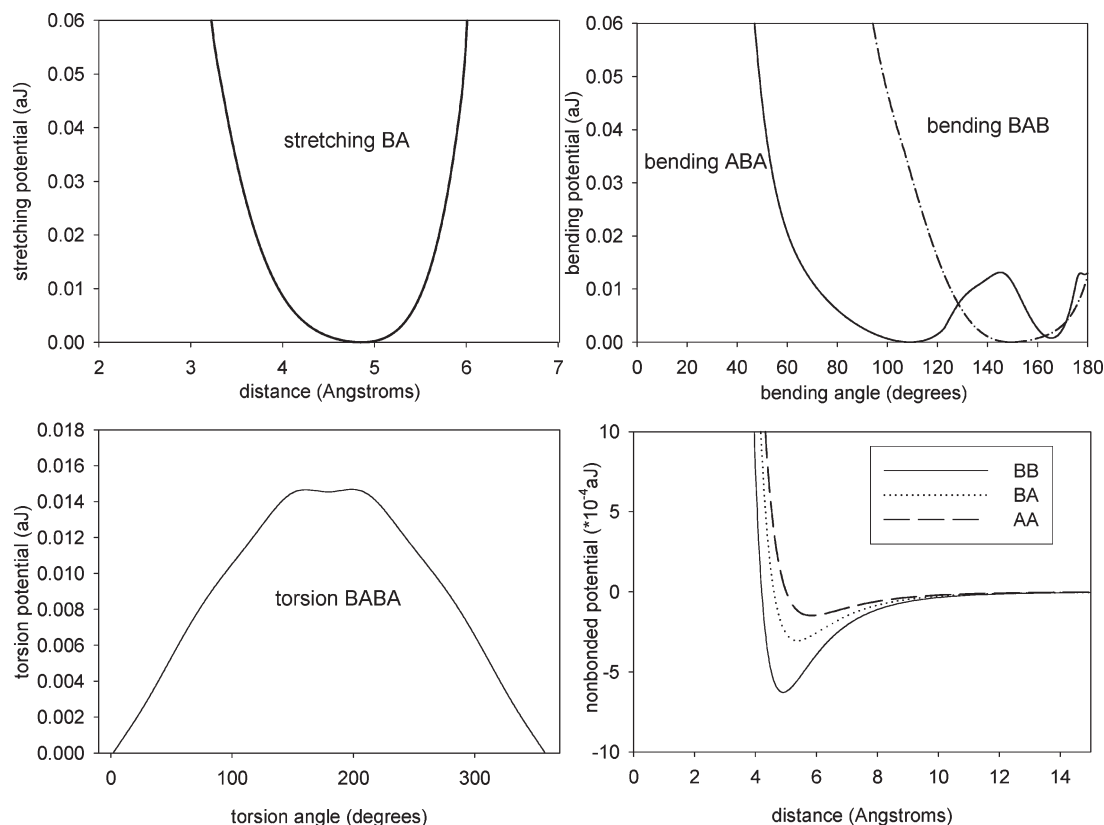
Figure 3. Bonded (stretching, bending, and torsion) and nonbonded CG potentials.

Table 3. Comparison of temperatures of CG beads of decamer from the equipartition theorem (ET) and from the Maxwell-Boltzmann distribution (MB) at $p = 0.13$ kPa, $T = 563$ K

species	$(T_x)^{ET}$	$(T_x)^{MB}$	$(T_x)^{Diff}$(%)	$(T_y)^{ET}$	$(T_y)^{MB}$	$(T_y)^{Diff}$ (%)	$(T_z)^{ET}$	$(T_z)^{MB}$	$(T_z)^{Diff}$ (%)	$(T_{avg})^{ET}$	$(T_{avg})^{MB}$	$(T_{avg})^{Diff}$ (%)	$(T_{avg})^{total}$
A	563	563	0.00	566	564	0.35	566	571	0.88	565	566	0.18	563.603
B	562	564	0.36	562	563	0.18	563	563	0.00	562	563	0.18	

distributions are also reported in the work of Hamandaris et al.[18] on polystyrene. We believe this similarity is due to a common treatment of phenol rings in the three CG models. The nonbonded BB, BA, and AA distributions show multiple peaks with the first peak centered at 5.0 Å. Figure 2 also shows that both bonded and nonbonded distributions are not significantly changing with DP, which indicates that our proposed CG model is able to capture the structural features of PET chains with different chain lengths. Any discrepancy based on chain length is probably due to end effects, which will diminish as we explore longer chains. We obtained the bonded stretching, bending and torsion CG potentials through eq 1, based on the bonded distribution functions of the decamer. The distribution functions of the decamer from atomistic simulation also serve as the target distributions, which we will compare later with the distribution functions from CGMD simulations of the decamer.

In Figure 3, we plot the bonded and nonbonded CG potentials of different interaction modes extracted from the PCFs of the atomistic simulation of the decamer. The bonded potentials are generated via eq 1 and the nonbonded potentials are generated using the $OZPY^{-1}$ procedure. The bonded potentials are shifted to have zero energy at the minima. The three nonbonded interaction potentials obtained from $OZPY^{-1}$ method are shown in Figure 3. These nonbonded potentials are close to Lennard-Jones 7−6 potential. Therefore, the calculated potentials were fit to a LJ 7−6 form to avoid (i) numerical noise and (ii) deficiencies

due to the approximate nature of the Percus−Yevick equation. These deficiencies include a softer repulsive potential resulting in greater overlap than observed in the atomistic simulations and an overestimation of the rate at which the potential rises at separations immediately beyond the first minimum. The specific procedure to obtain these nonbonded interaction potentials are presented in the Supporting Information. Note here that the nonbonded potentials are used in both intramolecular and intermolecular parts. Clearly, the nonbonded potential indicates the strongest interaction between two B beads, and the weakest interaction between two A beads. We can attribute this to the polar nature of the fragments in the B beads and the nonpolar nature of the benzene ring in the A bead.

Because we have simulated the chains with DP = 4, 6, 8, and 10 using both atomistic and CG simulations, there are a variety of properties that can be evaluated to determine the validity of the coarse-graining procedure. First, the equipartition of energy was checked. In both the atomistic and CG simulations, the average system temperature of a MD simulation is calculated based on the equipartition theorem, but it can also be computed by measuring the velocity distribution and fitting it to a Maxwell−Boltzmann distribution. For the CG simulation of the decamer, we computed the temperature of the A and B beads in the simulation in the x, y, and z dimensions using both procedures. The results are shown in Table 3 and Figure 4. The CG simulation results show that the average temperature equals to the set temperature with
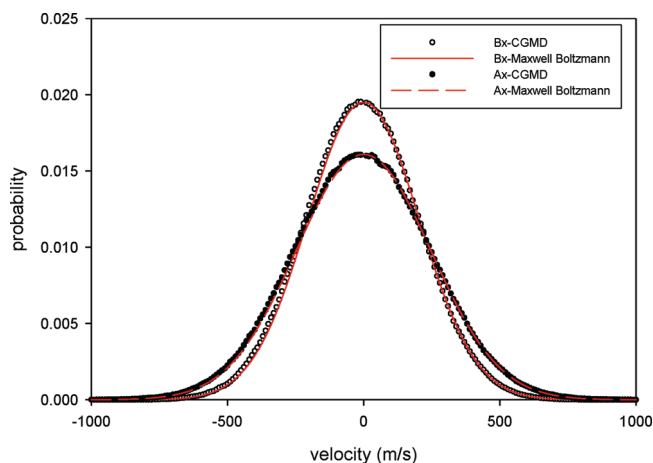
Figure 4. Comparison of *x*-direction velocity distribution of CG beads from CGMD simulation (data points) and the fitting of velocity distribution data to the Maxwell−Boltzmann distribution (line). The temperature can be extracted and compared with that of CGMD. Temperatures for all directions are shown in Table 1.

0.2% standard deviation. The Figure 3 shows the velocity distribution of CG beads B and A in the x direction, compared to the expected Maxwell−Boltzmann distribution based on the target temperature and fragments masses. Thus, in our CG simulations, we confirm both the equipartition of energy and the Maxwell−Boltzmann distribution of velocities. Consequently, the temperature of these CG simulations is well established. In fact, the equipartition theorem could be violated in CGMD simulations when the mass ratio of CG beads is very large. The mass ratio of the two CG beads (B/A) in our PET model is 1.45, closer to 1 than that in the polystyrene models (6.5 and 2.8) of Harmandaris et al.,[13,18] in which the mass was assumed to be evenly distributed between two CG beads to use a larger step size. Their later work shows that this assumption affects the scaling factor of dynamic properties.[13] On the basis of the above analysis, we avoided this assumption.

The second check between the atomistic and CG simulations that can be done is based on a comparison of the bonded PDFs. Equation 1, which is used to generate the bonded potentials, is subject to the assumption that all the interactions are independent of each other. The above potentials can only correctly reproduce the conformational sampling of atomistic description if all degrees of freedom are uncorrelated.[16] Villa et al.[16] and Harmandaris et al.[13,18] discuss the validation of this assumption. In Figure 5, we present the comparisons of all the bonded PDFs from atomistic MD and CGMD simulations of the decamer. The stretching, bending, and torsion PDFs agree reasonably well between the two techniques. All of the peaks are present. The largest discrepancy occurs in the ABA bending distribution, in which the CGMD results under-predict the population of the smaller peak at about 170°. We have validated the assumption of independence of the bonded modes through direct comparison of the distribution from the atomistic and CG simulations. Further understanding of the statistical interdependencies of different interaction modes could be achieved through additional analysis described in the literature.[13,16,30]

The third check between the atomistic and CG simulations that can be done is based on a comparison of the nonbonded PCFs and is a validation of the OZPY^{-1} coarse-graining procedure. The nonbonded distributions BB, BA and AA from CGMD also match the targets well. This indicates that the calculated CG potentials are able to reproduce the

structural features of PET chain at CG level. To further test this, we also compared the distributions of hexamer and octamer from CGMD with the atomistic PCFs, and found equivalent agreement (not shown). As presented elsewhere in most CG level simulation work,[6,13,18,27] one of the most important points of validation of the CG process is the reproduction of conformations from atomistic sampling. Having done this, we can further investigate the other physical properties from the CG simulations.

In Figure 6, we show snapshots from the CGMD simulations. All of these snapshots are taken from the equilibrium ensemble. In Figure 6a all molecules are shown to make it clear that we are simulating a dense melt. In parts b−f of Figures 6, all but five chains are rendered invisible to better indicate the shape of the chains. These structures are available to view and download at an archived site.[50]

In Figure 7, we show the distribution of chain end-to-end distance for DP = 10, 20, 30, 40, and 50. The end-to-end distance is defined as the distance between the two end BB groups. The end-to-end curve of the decamer displays two peaks. The peak centered at 4.5 Å corresponds to a folded configuration, as shown in Figure 6(b). The folded structure in PET oligomers has been reported by the other simulation work of PET.[5,51] The broader peak extending from 7 to 50 Å, with a maximum at 28.3 Å corresponds to the unfolded conformation. The end-to-end distribution of the decamer from atomistic MD simulation is also presented in Figure 7 (solid black line). The comparison is excellent. As DP increases, the qualitative two-peak behavior of the decamer disappears and the distribution becomes more Gaussian-like,[6] as shown for DP = 50. As expected, the position of the maximum in the peak increases with DP and the breadth of the curve increases with DP. The average end-to-end distance increases with DP, as can be seen in Table 1.

Figure 8 shows that the average chain end-to-end distance and radius of gyration as a function of DP in a log−log plot. Note here the results for tetramer, hexamer, octamer and decamer from atomistic MD simulations are also shown (open circle with back error bar). The lengths associated with the GCMD simulations are consistently slightly smaller than those of the atomistic MD simulations, because the beads are located at fragment center-of-masses. The polymer's structure and dynamic properties have the following chain length or molecular weight dependence.

$$X = a(DP)^b \qquad (8)$$

Here X is a property related to DP via the scaling exponent, b. The values of b for various properties as a function of chain length and degree of model resolution are listed in Table 4. Both structural measures can be well fit by eq 8. The scaling exponents for the radius of gyration and the chain end-to-end distance are 0.594 and 0.571, respectively, for DP up to 10 and 0.510 and 0.501 for DP from 20 to 40. Laso and Karayiannis[52,53] studied the scaling behaviors of oligomer systems, and found very similar values (0.58−0.60) for the scaling exponents are obtained in the whole range of volume fractions from dilute up to very dense samples suggesting universal character in the scaling behavior of oligomers. Indeed the value of 0.59 corresponds to specific folded (ring-like) and extended chain configurations that, because of their small size, markedly deviate from Gaussian coils. In a melt of sufficiently long PET chains, chains should behave as random walks and the exponent should be close to 0.5 as shown by Kamio et al.[6] Our scaling exponents of R_{ete} and R_g for longer chain systems (for DP greater than 20) are close to 0.5, which indicates that for DP greater than 20, the systems
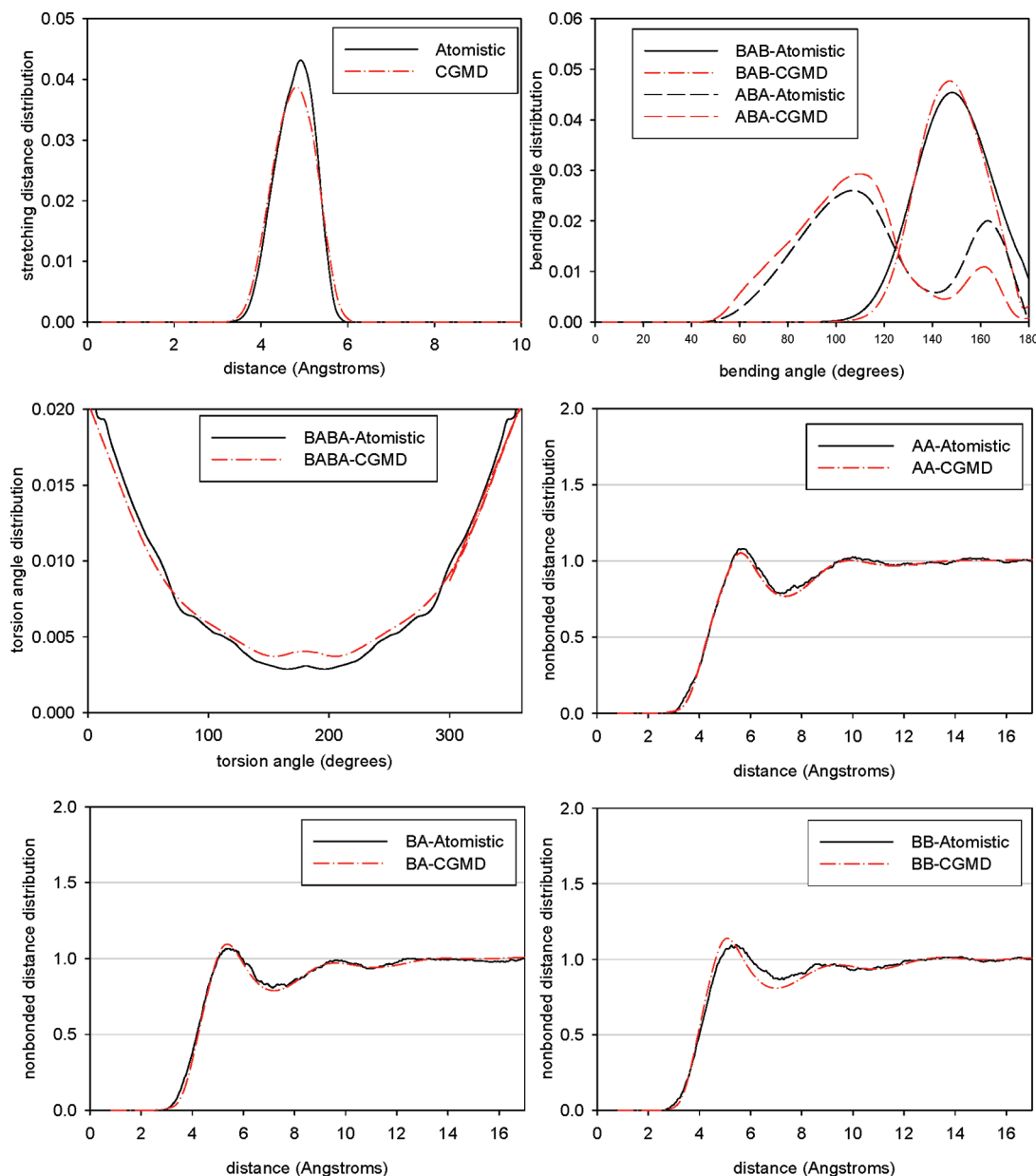
Figure 5. Comparisons of bonded (stretching, bending, and torsion) CG probability distribution functions (PDFs) and nonbonded CG pair correlation functions (PCFs) of decamer from atomistic MD simulation (target) and CGMD simulation.

become entangled. Indeed, the critical entangled molecular weight (M_e) of PET (3500 g/mol)[54] is between the molecular weight of decamer (1901 g/mol) and DP = 20 (3802 g/mol). The molecular weight of the highest DP (DP = 50) system is (9505 g/mol) 2.7 times of M_e. Therefore, a transition from Rouse like behavior to reptation behavior is possible. We will refer this issue back during the discussion of entanglement analysis.

Parts a and b of Figure 9 show the normalized chain end-to-end vector autocorrelation functions changing with observation time for the tetramer, hexamer, octamer and decamer systems. In Figure 9a, the black lines represent data from atomistic MD simulation using the molecular model, while the red lines represent values scaled from CGMD simulations using our CG model. The autocorrelation functions all decay to zero, which means the chains are fully relaxed. The atomistic simulations do not extend out as far as the CGMD simulations simply due to restrictions in computational resources. Thus, the benefits of applying the CG

procedure are evident. Note here the observation time was scaled.

We can extract useful information from the end-to-end vector autocorrelation function. By fitting this data to the exponential model or the KWW model[55] (a stretched exponential), one can extract chain relaxation times, $\tau_R{}^*$ and $\tau_{kww}{}^*$ respectively. These times correspond to the longest rotational relaxation time. The relaxation times and the stretching exponent, $\beta_{KWW}{}^*$, are reported in Table 1. As shown in Figure 9b, the fits to KWW model are reasonably good for DP equals 20, 30, 40, and 50. The relaxation times from the Rouse and the KWW model deviate at short chain length but agree relatively well for long chain length. The relaxation times increase strongly with DP. On the basis of chains with DP of 20, 30, 40, and 50, the scaling exponent b for $\tau_{kww}{}^*$ is 3.7. The scaling exponent obtained for the DP = 1 to 10 from the atomistic simulations was 2.78. Since there is a statistically significant change in the exponent from short to long chains, it is possible that this is a consequence of
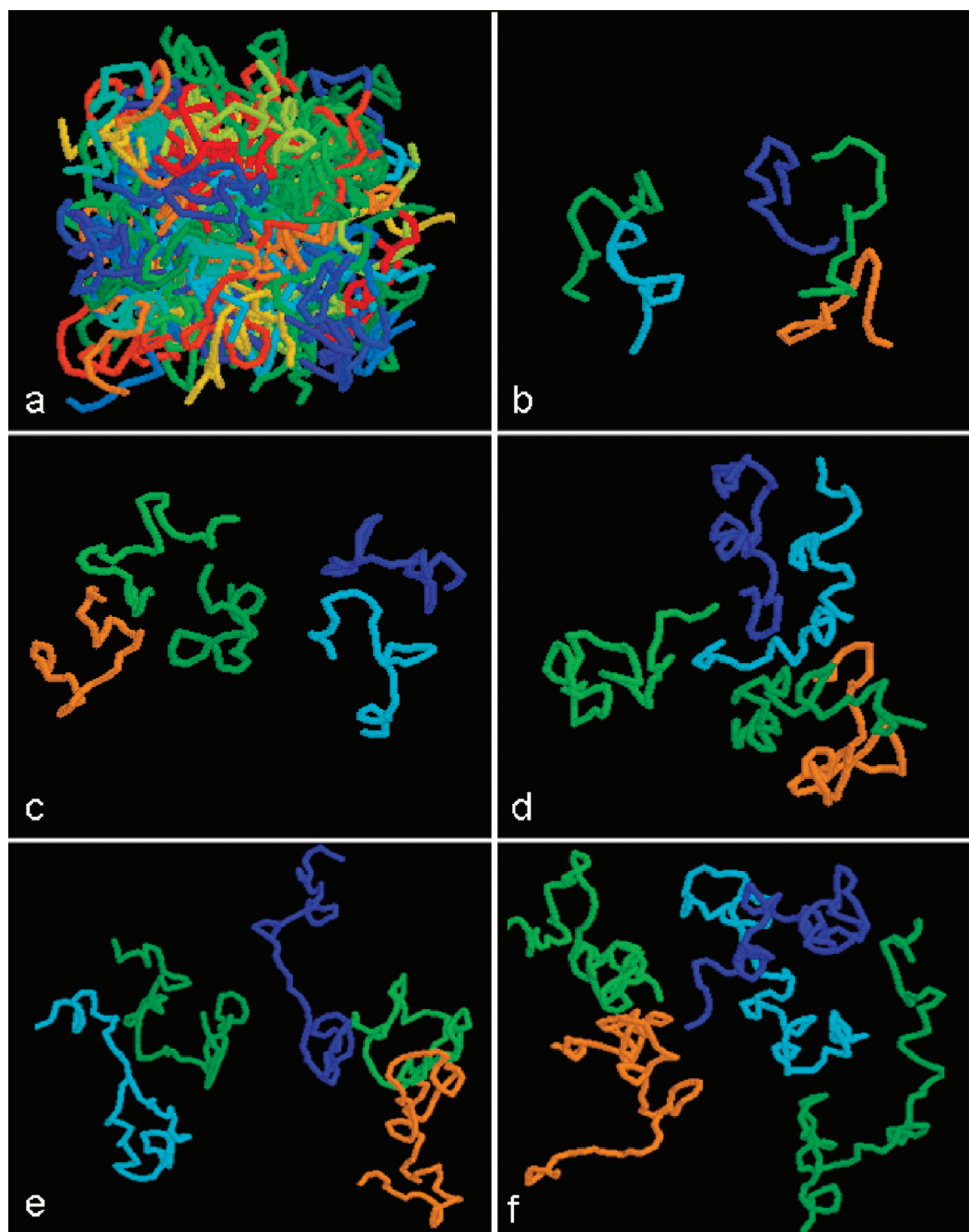
Figure 6. Snapshots of equilibrium configurations from CGMD simulations at $T = 563$ K, $p = 0.13$ kPa. (a) DP = 10, all molecules shown; (b–f) PET with different chain length (DP), selected molecules; (b) DP = 10; (c) DP = 20; (d) DP = 30; (e) DP = 40; (f) DP = 50.

moving from an unentangled to an entangled regime. As a point of reference, the Rouse model predicts a scaling exponent of 2 and reptation theory predicts a scaling exponent of 3.[56]

Another important issue investigated on the analysis of end-to-end vector autocorrelation functions is the scaling factor of relaxation times from atomistic MD and CGMD simulation of the tetramer, hexamer, octamer and decamer. We obtained two sets of relaxation times, τ_{kww} (from atomistic MD), which are listed in Table 2, and $\tau_{kww}*$ (from CGMD), which are listed in Table 1. The average of the ratio of $\tau_{kww}/\tau_{kww}*$ of tetramer, hexamer, octamer, and decamer is 7.5. In other words, the polymers relax on average 7.5 times faster in the CGMD simulation than they do in the atomistic simulation. This is because fewer degrees of freedom are used

in the CG model, which accordingly causes faster dynamics in the CGMD simulation than the full atomistic MD simulation.[13] This scaling factor is reported in the top row of Table 2. As a point of clarification, note that we now have scaling *exponents* relating the behavior of a property to degree of polymerization and scaling *factors*, providing proportionalities between properties of the CGMD simulations to those of the atomistic MD simulations.

We also report the kinetic, bonded potential (stretching, bending and torsion) and nonbonded potential (intramolecular and intermolecular) energies in Table 1 (raw data) and Table 2 (scaled data). These energies are reported in units of aJ/bead. The scaling factors reported in Table 2 were generated by calculating the average ratio of the property from CGMD and atomistic simulations. The use of a single constant

for scaling the kinetic energy across all DP is excellent, as can be judged by comparison of the scaled energies from
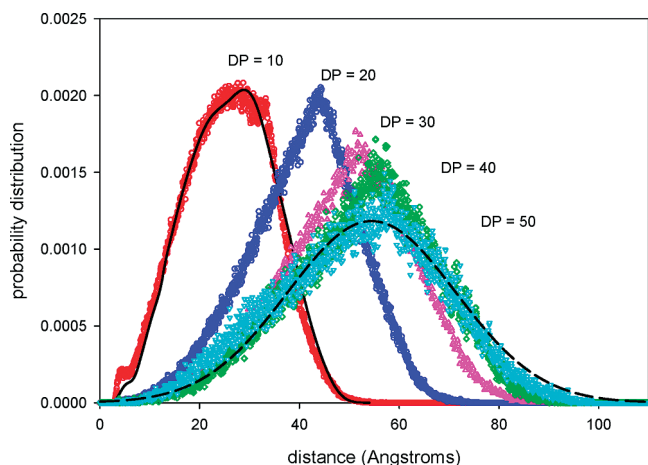

Figure 7. Comparisons of the chain end-to-end distance probability distributions for DP = 10, 20, 30, 40, and 50 from CGMD. For DP = 10, the solid line represents the distribution from atomistic MD simulation. For DP = 50, the dash line represents the distribution predicted by Gaussian function.
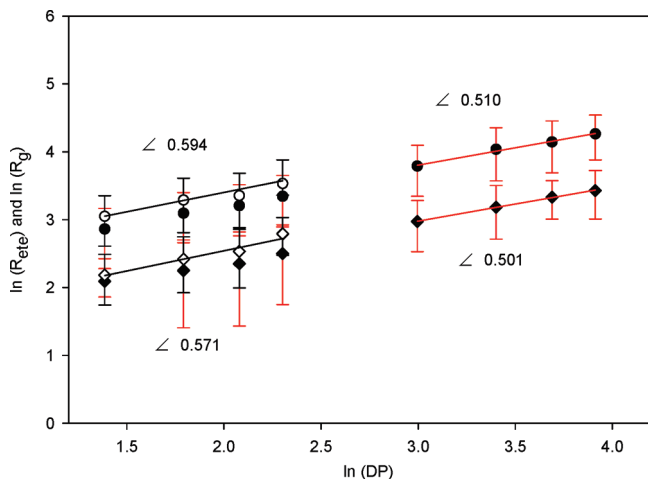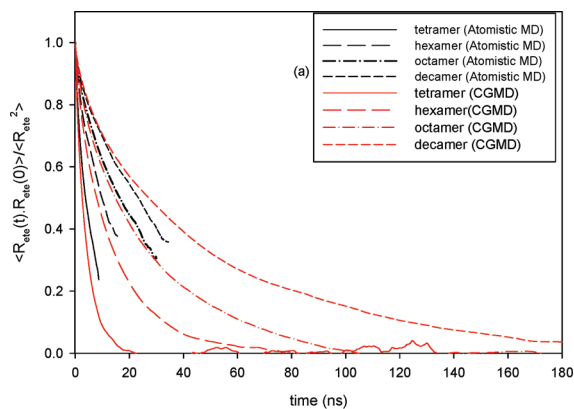

Figure 8. Average chain end-to-end distance (R_{ete}, circles) and radius of gyration (R_g, diamonds) as a function of DP from atomistic MD (open symbols) and CGMD (solid symbols). The error bars are one standard deviation. Linear regressions of the MD data (short chains) and CGMD data (long chains) are shown with the slope reported.

atomistic and CGMD simulation in Table 2. The scaling for the potential energies is reasonably good with an average error of 6.2% and 2.2% for the bonded and nonbonded terms, respectively. These scaling factors for the energies allow one to compute thermodynamic properties, such as the internal energy, of the atomistic chain from the CGMD simulation.

3.2. Transport Properties. In this section, we report the self-diffusivity (D) and zero-shear rate viscosity (η) as a function of DP. The self-diffusivity is obtained from the mean-square displacements (MSD) through Einstein's equation given as

$$D = \frac{1}{6} \lim_{t \to \infty} \frac{1}{t} \langle [r_{cm}(t) - r_{cm}(0)]^2 \rangle \tag{9}$$

where r_{cm} is the center of mass position of the chain.

In Figure 10, we plot the mean square displacement versus observation time on a log−log plot. In order to satisfy the infinite time limit, the slopes of the curves must be unity. These slopes are reported in the legend of Figure 10 and are all very close to unity. This is evidence that the simulations have been run sufficiently long to achieve valid self-diffusivities. The numerical values of the self-diffusivities from CGMD simulation are reported in Table 1. We acknowledge that it is likely that the statistical accuracy of the estimate diminishes as the chain length increases due to the fact that we have not been able to simulate for as many relaxation times with the long chains as we did with the short chains. This is reflected in the uncertainties reported in Table 1 where the standard deviation is 19% for DP = 10 and 40% for DP = 50. Scaled values are plotted in Figure 11 as a function of DP. The self-diffusivity decreases with DP as expected. The scaling exponent for the self-diffusivity for DP = 20 to 50 is −2.00. The scaling exponent obtained for DP = 4 to 10 is −1.91, which can be compared to the DP = 1 to 10 from the atomistic simulations, which was −2.01.[5] Since this exponent changes very little from short to long chains, it is not a useful measure of degree of entanglement. As a point of reference, the

Table 4. Scaling Exponents for Various Properties As a Function of Chain Length and Degree of Model Resolution

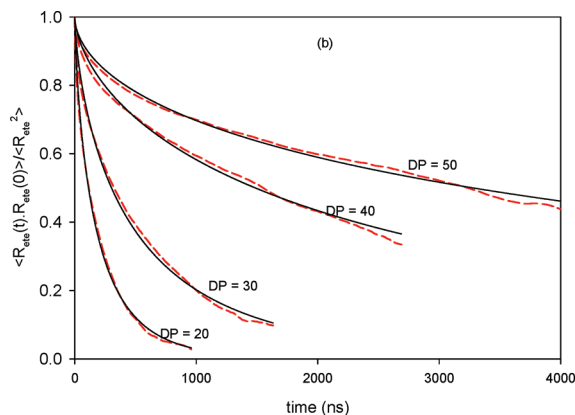| DP	simulation method	D	η	τ_{KWW}	$\langle R_{ete} \rangle$	$\langle R_g \rangle$
1−10	atomistic MD	−2.01	0.96	2.78	0.594	0.571
4−10	atomistic MD	−1.91	1.6	2.81	0.59	0.57
20−50	CGMD	−2.0	2.0	3.7	0.51	0.50
Rouse model	N/A	−1	1	2	0.59	0.59
reptation model	N/A	−2	3	3	0.50	0.50

Figure 9. (a) Comparison of the end-to-end distance autocorrelation functions for the tetramer, hexamer, octamer and decamer from atomistic MD and CGMD simulations (with time scaled). (b) End-to-end distance autocorrelation function and its fitting to the KWW model for DP = 20, 30, 40, and 50 from the CGMD simulations.
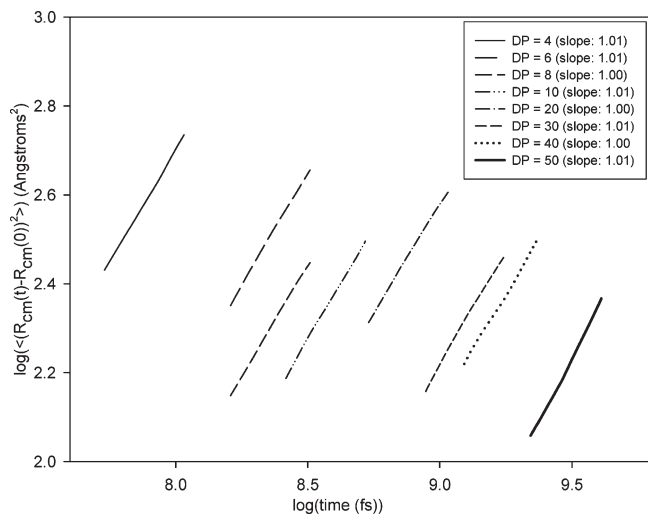
Figure 10. Mean square displacement of chain center of mass as a function of observation time for all DPs. The slope reported in the legend should be unity to satisfy the long-time limit of the Einstein relation.
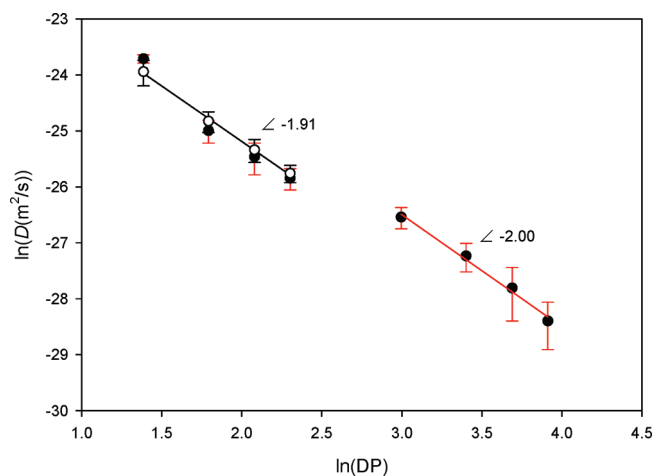

Figure 11. Average self-diffusivity (*D*) as a function of DP from atomistic MD (open symbols) and CGMD (solid symbols). The error bars are one standard deviation. Linear regressions of the MD data (short chains) and CGMD data (long chains) are shown with the slope reported.

theoretical prediction of the scaling exponent from reptation theory for entangled polymer melts is -2. We do not observe any behavior predicted by the Rouse model (for which $b = -1.0$) for any chain lengths. Indeed, it has been reported in the literature that the dynamic properties deviate from the Rouse model for short-chain unentangled polymer systems.[57] This is attributed to the presence of chain stiffness, nonbonded interactions, and chain uncrossability, which are not accounted for by the Rouse model.[57]

If we compare the numerical values of the diffusivities from atomistic simulations (Table 2) and CGMD simulations (Table 1) for chains with DP of 4, 6, 8, and 10, we find that the average ratio of diffusivities (CG over atomistic) is 0.186. (The diffusivities in Figure 11 are scaled by this number.) The inverse of this is 5.38. In other words, diffusion is occurring 5.38 times faster in the CGMD simulation than in the atomistic MD simulation. Recall that the polymer relaxed 7.5 times faster in the CGMD simulation based on an analogous comparison of τ_{kww}. One might have expected these numbers to be the same. At this point, we do not have a complete explanation for the discrepancy. The use of a time
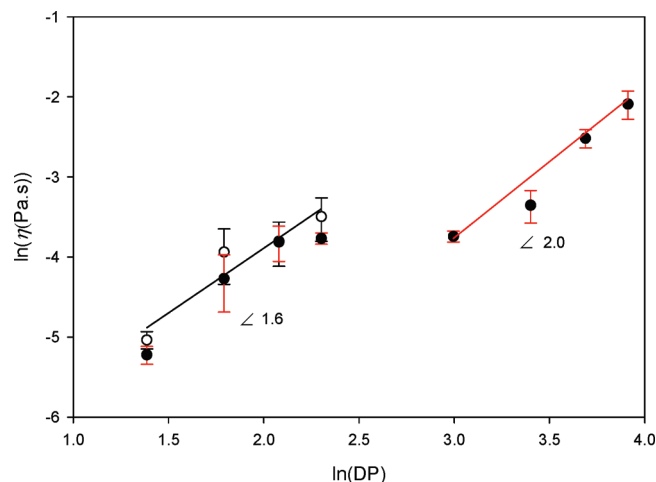

Figure 12. Average zero-shear-rate-viscosity (η) as a function of DP from atomistic MD (open symbols) and CGMD (solid symbols). The error bars are one standard deviation. Linear regressions of the MD data (short chains) and CGMD data (long chains) are shown with the slope reported.

scaling constant has only an empirical basis. The different dynamic properties (relaxation time, diffusivity, viscosity) represent mechanisms of entropy generation. Because the entropy of the atomistic and coarse-grained models are different, it may well turn out that the use of a single time-scaling constant gives only a first order approximation of the diverse effects of a more complicated issue. However, in Table 2, when we provide the scaled properties from the CGMD simulations to compare with the atomistic MD simulations, we provide all of the scaling factors in the top row of the table.

The zero-shear-rate viscosity is based on time integration of the momentum autocorrelation function

$$\eta_{xy} = \frac{1}{V k_B T} \int_0^\infty \langle \sigma_{xy}(t)\sigma_{xy}(0) \rangle \, dt \qquad (10)$$

where σ_{xy} is the xy component of the stress tensor defined to have a potential and kinetic contribution

$$\sigma_{xy} = \frac{1}{2} \sum_{i=1}^N \sum_{j \neq i}^N F_{ijx} r_{ijy} + m_i \sum_{i=1}^N u_{ix} u_{iy} \qquad (11)$$

where r_{ijx} and F_{ijx} are respectively the separation and force between particles i and j in the x dimension, m_i is the mass of particle i.

Following a previously tested procedure,[5,58] we obtained numerical values of the zero-shear-rate viscosities from the CGMD simulations, which are given in Table 1. Scaled values are plotted in Figure 12 as a function of DP. The scaling exponent for the zero shear rate viscosity for DP = 20 to 50 is 2.0. The scaling exponent obtained for DP = 4 to 10 is 1.6, which can be compared to the DP = 1 to 10 from the atomistic simulations, which was 0.96.[5] The values deviate from the theoretical prediction ($b = 1$ for the Rouse model and $b = 3.0$ for the reptation model). The deviation from Rouse model is expected[57,59] due to the reasons mentioned above. The exponent for short chains $b = 1.6$ is close to the finding of other simulation work ($b = 1.8$[60] and $b = 1.5$[57]). For entangled long chain systems, the exponents $b = 3.6$[60] and $b = 3.2$[57] have been observed.

To map zero-shear-rate viscosity from CGMD simulation back to the molecular level, we again calculate an average scaling factor between the viscosities of the CGMD and

Table 5. Calculated Properties from Z Algorithm for DP = 10, 20, 30, 40, and 50 Systems at p = 0.13 kPa, T = 563 K

DP	$\langle L_{pp} \rangle$ (Å)	d (Å)	N_e	Z	N_{ES}
10	31.99	19.07	8.82	1.87	7.19
20	62.08	33.08	14.60	2.44	11.16
30	92.17	35.38	18.67	3.51	13.48
40	110.22	38.49	22.16	4.34	15.13
50	133.23	34.74	22.60	6.02	14.37
rheology models	N/A	35,[68] 38−43[66]	30.2,[68] 24.2,[66] 25.0[67]	N/A	N/A

atomistic MD simulations for DP = 4, 6, 8, and 10. The average ratio is 6.62. If we invoke the Stokes−Einstein (SE) relation,[61,62] which according to hydrodynamic theory applies well to the diffusion of large spherical molecules in solvent of low molecular weight (admittedly not the system here), then

$$\frac{D\eta}{k_B T} = \frac{1}{4\pi R_{SE}} \tag{12}$$

where R_{SE} is the particle size. R_{SE} can also be represented by the chain radius of gyration (R_g). Thus, according to the Stokes−Einstein relation, the scaling factor for viscosity is simply the inverse of the scaling factor the diffusivity (since we have assumed a scaling of 1 for the radius of gyration), which is 5.38. The values of the viscosity in Table 2 and Figure 12 have been scaled by 5.38. There is relatively good agreement between the viscosities from the CGMD and atomistic MD simulations. There is scatter in the data, (as is typical for zero shear rate viscosities obtained in this way), but no systematic discrepancy.

We would like to better understand the degree of entanglement in these systems. As we mentioned above, the actual molecular weight of DP = 20 systems has exceeded the entanglement molecular weight of PET. The scaling exponents for the end-to-end distance, radius of gyration and the slowest relaxation time showed a statistically significant decrease when moving from short chains (DP ≤ 10) to longer chains (DP ≥ 20). However, the scaling exponent for the self-diffusivity did not show any statistically significant change between short and long chains.

3.3. Entanglement Analysis. A clearer understanding of entanglement can emerge from a more geometric approach in which one extracts entanglement information directly from configurations of the chains. To this end, we analyzed snapshots of DP = 10, 20, 30, 40, and 50 systems using the Z-code.[45] The Z-code and CReTA package[63] are two common algorithms to study the entanglements in polymeric systems. Kamio et al.[6] studied the entanglements of long chain PET using the above two algorithms. The calculated quantities like primitive path length and entanglement spacing are in good agreement. In this work, we implement only the Z-code to study the entanglements in longer chain systems. The details of the Z-code and its application can be found elsewhere.[45,64,65] The calculated mean contour length of primitive path ($\langle L_{pp} \rangle$), tube diameter (d), number of monomers between entanglement points (N_e) and number of entanglements (Z) for PET with DP from 10 to 50 are listed in Table 5. These values were generated by averaging over 1000 snapshots distributed through-out the simulation, each containing 125 chains. The value of tube diameter is in good agreements with rheological data reported in the literature[66−68] for DP from 20 to 50. The average value is 35.42 (Å), which can be compared with the reported value of 35 (Å).[68] The difference is within 1.2%. The tube diameter for the DP = 10 system deviates from that of the other simulations and from reports in the literature, which may results from it being unentangled. The values of $\langle L_{pp} \rangle$ for entangled systems are lower than that reported by Kamio

et al.[6] This is probably because a longer chain length used in their work. It has been shown that the value of $\langle L_{pp} \rangle$ increases with chain length.[64] To further compare our results with the literature, we also reported the values of interentanglement strand length (N_{ES}) in Table 4. N_{ES} is defined as[6]

$$N_{ES} = \frac{N(N-1)}{Z(N-1) + N} \tag{13}$$

where N is the number of beads in a chain. The average value for DP from 20 to 50 is 13.59 ± 1.63, which is in agreements with that reported in the literature,[6] in which the value from CReTA is 13.87 and from Z is 14.9. The slight dependence of N_{ES} on DP may be due to differences in the densities. The agreement of the tube diameter and N_{ES} comparisons also indicates that good equilibration of the melt topological structure has been achieved, which is further verified by the fact that no significant difference is observed on these the statistical properties from the analysis of multiple configurations taken at different times.

4. Conclusions

A coarse-grained (CG) model of poly(ethylene terephthalate) (PET) was developed and implemented in CG molecular dynamics (MD) simulations of PET chains with degree of polymerization up to 50. The CG potential is parametrized to structural distribution functions obtained from atomistic simulations[5] using an inversion procedure based on the Ornstein−Zernike equation with the Percus−Yevick approximation (OZPY).[29] The CGMD simulation of PET chains satisfactorily reproduces the structural and dynamic properties from atomistic MD simulation of the same systems. From the CGMD simulations, we obtained structural and transport properties for PET with degrees of polymerization from 4 to 50 at the industrially relevant state point (T = 563 K, p = 0.13 kPa).

Scaling exponents are reported for five properties as a function of DP: the end-to-end distance, the radius of gyration, longest rotational relaxation time, the self-diffusivity and the zero shear rate viscosity. We calculated scaling exponents for both short chains (DP ≤ 10) and longer chains (DP ≥ 20). We observed that the scaling exponents for the end-to-end distance, the radius of gyration, longest rotational relaxation time and the zero shear rate viscosity show a statistically significant different between short and long chains. However, the scaling exponent for the self-diffusivity did not show any statistically significant change between short and long chains. The exponents for long chains for the end-to-end distance, the radius of gyration and the self-diffusivity are in good agreement with predictions from reptation theory. The exponents for the viscosity fall between the Rouse model and reptation theory for both short and long chains. The exponents for the longest rotational relaxation time exceed the Rouse model and reptation theory for both short and long chains, respectively.

In an effort to understand how dynamic properties from CGMD simulations can be scaled, we compared CGMD and atomistic MD simulations of PET for DP up to 10. Comparison of structural properties, such as end-to-end distance or radius of gyration, show that no length scaling is necessary. Using the

longest rotational relaxation time as a standard, we find that the time scaling factor in the CGMD simulations is 7.5. However, using the self-diffusivity as the standard, the time scaling factor is 5.38. The viscosity yields a scaling factor of 6.22.

The entanglement analysis, using the Z-code,[45] shows that for DP = 20 to 50, tube diameter (d), number of monomers between entanglement points (N_e) and interentanglement strand length (N_{ES}) are very close to the reported values for entangled PET melts. For DP = 50, there are on average six entanglements per chain. Thus, we have at least a partially entangled system for the longer chains, explaining some of the intermediate scaling exponents observed in the simulations.

Supporting Information Available: Text describing in detail the $OZPY^{-1}$ procedure for polymers including tables of necessary combinations.This material is available free of charge via the Internet at http://pubs.acs.org.

References and Notes

(1) Kremer, K. *Macromol. Chem. Phys.* **2003**, *204*, 257–264.
(2) Hedenqvist, M. S.; Bharadwaj, R.; Boyd, R. H. *Macromolecules* **1998**, *31*, 1556–1564.
(3) Bharadwaj, R. K.; Boyd, R. H. *Polymer* **1999**, *40*, 4229–4236.
(4) Boyd, S. U.; Boyd, R. H. *Macromolecules* **2001**, *34*, 7219–7229.
(5) Wang, Q. F.; Keffer, D. J.; Petrovan, S.; Thomas, J. B. *J. Phys. Chem. B* **2010**, *114*, 786–795.
(6) Kamio, K.; Moorthi, K.; Theodorou, D. N. *Macromolecules* **2007**, *40*, 710–722.
(7) Karayiannis, N. C.; Mavrantzas, V. G.; Theodorou, D. N. *Macromolecules* **2004**, *37*, 2978–2995.
(8) Pavel, D.; Shanks, R. *Polymer* **2003**, *44*, 6713–6724.
(9) Cail, J. I.; Stepto, R. F. T.; Taylor, D. J. R.; Jones, R. A.; Ward, I. M. *Phys. Chem. Chem. Phys.* **2000**, *2*, 4361–4367.
(10) Saunders, L. S.; Ward, I. M.; Cail, J. I.; Stepto, R. F. T. *Polymer* **2004**, *45*, 2357–2366.
(11) Tonelli, A. E. *J. Polym. Sci., Part B: Polym. Phys.* **2002**, *40*, 1254–1260.
(12) Eslami, H.; Muller-Plathe, F. *Macromolecules* **2009**, *42*, 8241–8250.
(13) Harmandaris, V. A.; Reith, D.; Van der Vegt, N. F. A.; Kremer, K. *Macromol. Chem. Phys.* **2007**, *208*, 2109–2120.
(14) Chen, C. X.; Depa, P.; Maranas, J. K.; Sakai, V. G. *J. Chem. Phys.* **2008**, *128*, 124906.
(15) Lyubimov, I. Y.; McCarty, J.; Clark, A.; Guenza, M. G. *J. Chem. Phys.* **2010**, *132*, 5.
(16) Villa, A.; Peter, C.; van der Vegt, N. F. A. *Phys. Chem. Chem. Phys.* **2009**, *11*, 2077–2086.
(17) Voltz, K.; Trylska, J.; Tozzini, V.; Kurkal-Siebert, V.; Langowski, J.; Smith, J. *J. Comput. Chem.* **2008**, *29*, 1429–1439.
(18) Harmandaris, V. A.; Adhikari, N. P.; van der Vegt, N. F. A.; Kremer, K. *Macromolecules* **2006**, *39*, 6708–6719.
(19) Harmandaris, V. A.; Kremer, K. *Macromolecules* **2009**, *42*, 791–802.
(20) Chen, L. J.; Qian, H. J.; Lu, Z. Y.; Li, Z. S.; Sun, C. C. *J. Phys. Chem. B* **2006**, *110*, 24093–24100.
(21) Chen, C. X.; Depa, P.; Sakai, V. G.; Maranas, J. K.; Lynn, J. W.; Peral, I.; Copley, J. R. D. *J. Chem. Phys.* **2006**, *124*, 234901.
(22) Lee, H.; de Vries, A. H.; Marrink, S. J.; Pastor, R. W. *J. Phys. Chem. B* **2009**, *113*, 13186–13194.
(23) Sun, Q.; Faller, R. *J. Chem. Theory Comput.* **2006**, *2*, 607–615.
(24) Sun, Q.; Faller, R. *J. Chem. Phys.* **2007**, *126*, 144908.
(25) Hess, B.; Leon, S.; van der Vegt, N.; Kremer, K. *Soft Matter* **2006**, *2*, 409–414.

(26) Peter, C.; Delle Site, L.; Kremer, K. *Soft Matter* **2008**, *4*, 859–869.
(27) Reith, D.; Putz, M.; Muller-Plathe, F. *J. Comput. Chem.* **2003**, *24*, 1624–1636.
(28) Guenza, M. G. *J. Phys.: Condens. Matter* **2008**, *20*, 033101.
(29) Wang, Q.; Keffer, D. J.; Nicholson, D. M.; Thomas, J. B. *Phys. Rev. E* **2010**, *81*, 061204.
(30) Fritz, D.; Harmandaris, V. A.; Kremer, K.; van der Vegt, N. F. A. *Macromolecules* **2009**, *42*, 7579–7588.
(31) Curro, J. G.; Schweizer, K. S. *Macromolecules* **1987**, *20*, 1928–1934.
(32) Schweizer, K. S.; Curro, J. G. *Adv. Chem. Phys.* **1997**, *98*, 1–142.
(33) Schweizer, K. S.; David, E. F.; Singh, C.; Curro, J. G.; Rajasekaran, J. J. *Macromolecules* **1995**, *28*, 1528–1540.
(34) McCarty, J.; Lyubimov, I. Y.; Guenza, M. G. *J. Phys. Chem. B* **2009**, *113*, 11876–11886.
(35) Clark, A. J.; Guenza, M. G. *J. Chem. Phys.* **2010**, *132*, 044902.
(36) Yatsenko, G.; Sambriski, E. J.; Nemirovskaya, M. A.; Guenza, M. *Phys. Rev. Lett.* **2004**, *93*, 257803.
(37) Zhao, L.; Li, Y. G.; Mi, J. G.; Zhong, C. L. *J. Chem. Phys.* **2005**, *123*, 124905.
(38) Davis, H. T. *Statistical mechanics of phases, interfaces, and thin films*; VCH: New York, 1996.
(39) Lee, L. L. *Molecular thermodynamics of nonideal fluids*; Butterworths: Boston, MA, 1988.
(40) Law, A. D.; Buzza, D. M. A. *J. Chem. Phys.* **2009**, *131*, 094704.
(41) Silbermann, J. R.; Klapp, S. H. L.; Schoen, M.; Chennamsetty, N.; Bock, H.; Gubbins, K. E. *J. Chem. Phys.* **2006**, *124*, 074105.
(42) Behrens, S. H.; Grier, D. G. *Phys. Rev. E* **2001**, *6405*, 050401.
(43) Brunner, M.; Bechinger, C.; Strepp, W.; Lobaskin, V.; von Grunberg, H. H. *Europhys. Lett.* **2002**, *58*, 926–932.
(44) Rajagopalan, R.; Rao, K. S. *Phys. Rev. E* **1997**, *55*, 4423–4432.
(45) Kroger, M. *Comput. Phys. Commun.* **2005**, *168*, 209–232.
(46) Keffer, D. J.; Baig, C.; Adhangale, P.; Edwards, B. J. *Mol. Simul.* **2006**, *32*, 345–356.
(47) Tuckerman, M.; Berne, B. J.; Martyna, G. J. *J. Chem. Phys.* **1993**, *99*, 2278–2279.
(48) Feldman, D.; Barbalata, A. *Synthetic polymers: technology, properties, applications*; Chapman & Hall: London, 1996.
(49) Henderson, D.; Sokolowski, S. *J. Chem. Phys.* **1996**, *104*, 2971–2975.
(50) Keffer, D. J. *Molecular Simulation Structures from the Computational Materials Research Group at the University of Tennessee*; University of Tennessee: Knoxville, TN, 2010.
(51) West, S. M.; Smallridge, A. J.; Uhlherr, A.; Volker, S. *Macromol. Chem. Phys.* **2000**, *201*, 2532–2534.
(52) Laso, M.; Karayiannis, N. C. *J. Chem. Phys.* **2008**, *128*, 174901.
(53) Karayiannis, N. C.; Laso, M. *Macromolecules* **2008**, *41*, 1537–1551.
(54) Aharoni, S. M. *Makromol. Chem.—Macromol. Chem. Phys.* **1978**, *179*, 1867–1871.
(55) Tsolou, G.; Mavrantzas, V. G.; Theodorou, D. N. *Macromolecules* **2005**, *38*, 1478–1492.
(56) Tzoumanekas, C.; Lahmar, F.; Rousseau, B.; Theodorou, D. N. *Macromolecules* **2009**, *42*, 7474–7484.
(57) Lahmar, F.; Tzoumanekas, C.; Theodorou, D. N.; Rousseau, B. *Macromolecules* **2009**, *42*, 7485–7494.
(58) Keffer, D. J.; Edwards, B. J.; Adhangale, P. *J. Non-Newtonian Fluid Mech.* **2004**, *120*, 41–53.
(59) Padding, J. T.; Briels, W. J. *J. Chem. Phys.* **2002**, *117*, 925–943.
(60) Pearson, D. S.; Strate, G. V.; Vonmeerwall, E.; Schilling, F. C. *Macromolecules* **1987**, *20*, 1133–1141.
(61) Saalwachter, K.; Burchard, W. *Macromolecules* **2001**, *34*, 5587–5598.
(62) Das, S. K.; Horbach, J.; Binder, K.; Fisher, M. E.; Sengers, J. V. *J. Chem. Phys.* **2006**, *125*, 12.
(63) Tzoumanekas, C.; Theodorou, D. N. *Macromolecules* **2006**, *39*, 4592–4604.
(64) Kim, J. M.; Keffer, D. J.; Kroger, M.; Edwards, B. J. *J. Non-Newtonian Fluid Mech.* **2008**, *152*, 168–183.
(65) Shanbhag, S.; Kroger, M. *Macromolecules* **2007**, *40*, 2897–2903.
(66) Fetters, L. J.; Lohse, D. J.; Richter, D.; Witten, T. A.; Zirkel, A. *Macromolecules* **1994**, *27*, 4639–4647.
(67) Lorentz, G.; Tassin, J. F. *Polymer* **1994**, *35*, 3200–3205.
(68) Fetters, L. J.; Lohse, D. J.; Colby, R. H. In *Physical Properties of Polymers Handbook*; Mark, J. E., Ed.; Springer: New York, 2007.